The Role of Xantphos in forming an Elusive dirhodium-η^1-allyl Intermediate in a Rh(II)-Catalyzed Allylic Alkylation: A Combined Computational and Experimental Study

Anubhav Goswami,[a] Romin Gogoi,[a] Arpita Panda,[b] Aakash Chandresh Sheth,[a] and Garima Jindal*[a]

[a]Department of Organic Chemistry, Indian Institute of Science, Bangalore 560012 (India)

[b]Department of Inorganic and Physical Chemistry, Indian Institute of Science, Bangalore, 560012 (India)

email: gjindal@iisc.ac.in

Abstract

The use of dirhodium tetracarboxylate catalysts in multicomponent reactions involving allylic alkylation has been a formidable challenge to synthetic chemists. A unique strategy by means of catalyst structure modification in the presence of an external ligand, Xantphos, has recently enabled their efficient use in one-pot reactions involving carbene insertion into X–H bonds followed by allylic alkylation. However, the origin of the novel reactivity and the mechanism of such reactions remain unclear. Herein, we report a combined computational and experimental mechanistic study to shed light on the ligand-enabled catalyst structure modification and its implication in catalysis. This unique reactivity is enabled by the dissociation of an octanoate bridge driven by κ^2-Xantphos ligation to the dirhodium core of the catalyst. This in turn allows for a hitherto unknown oxidative addition with the Rh(II) catalyst resulting in a dirhodium-η^1-allyl species. For the first time, we confirm the presence of such a species in solution through *in situ* NMR and cyclic voltammetry experiments in line with DFT calculations. Alongside, we study the role of the base and solvent in generating the nucleophilic partner that can trap the electrophilic allylic species. This study is expected to guide future catalyst design, including chiral variants, for exploring newer modes of reactivity and selectivity using dirhodium catalysis.

1 Introduction

Dirhodium tetracarboxylate-based paddlewheel complexes have found widespread utility in the functionalization of X–H (X = N, O, S, C) bonds with impressive regio-, chemo-, and stereoselectivities.[1] The simple yet elegant two-component strategy has been further extended to MCRs (multicomponent reactions) where the reactive onium ylide intermediate traps an external electrophile. The capture of external electrophiles both in the form of Michael acceptors (prior to a delayed proton transfer) and electrophile transfer reagents or intermediates to yield valuable and diverse molecular scaffolds has been reported (Scheme 1).[2]

Despite the burgeoning success of dirhodium tetracarboxylate-based catalysts for X–H insertion reactions, the catalysts of choice for another class of reactions involving allylic alkylation via metal-allyl intermediates largely remain monorhodium- and palladium-based.[3] This is due to the ease of formation of these intermediates through a facile oxidative addition process, which is typically not possible in the stable dirhodium tetracarboxylate architecture owing to the lack of two vacant adjacent coordination sites. Hence, dirhodium tetracarboxylate-based catalysts are, by themselves, incapable of catalyzing the MCRs involving allylic reagents as electrophiles.[2k,l] The use of palladium or monorhodium complexes, which can, in principle, catalyze such an MCR alone, is limited by the rapid allylation which precludes X–H insertion.[4] These complications, therefore, generally necessitate the use of two metal catalysts, one for the formation of the metal carbene and the other for that of the metal-allyl complex.

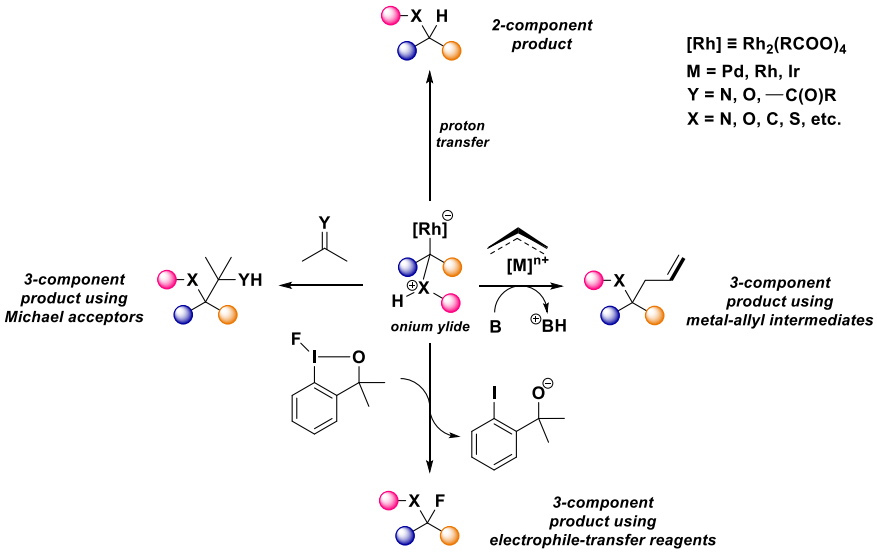

Scheme 1. Two- and three-component reactions catalyzed by dirhodium carboxylates.

Despite the challenges discussed above, Wang and co-workers have recently developed an MCR protocol for the construction of α-quaternary α-amino ester from an α-diazoester, amine, and allylic compound, involving a dirhodium tetracarboxylate/Xantphos-catalyzed carbene insertion and allylic alkylation relay (Scheme 2).[4] The unique reactivity resulted from a combination of different factors, including the nature of the catalyst, external ligand, base, and solvent. Their synthesis design was based on the possible modification of the catalyst in the presence of the external Xantphos ligand where the choice of the solvent and base also played a crucial role. The modification of dirhodium catalysts in different ways has enabled newer reactivity in several other reactions. For instance, chiral carboxylate ligands have been incorporated into the catalyst framework for the development of asymmetric X–H insertion reactions.[5] There have also been a number of attempts to tune the reactivity of dirhodium-based catalysts by using external and tethered axial ligands without modifying the paddlewheel framework.[6] Although the use of external chiral ligands in this aspect has only resulted in modest enantioselectivities so far, the differential reactivities are of immense importance.[6b] In the work by Wang and coworkers, it was hypothesized that the external Xantphos ligand drives the dissociation of one of the carboxylate ligands. This in turn

provides vacant adjacent sites necessary for the oxidative addition of the allyl substrate, resulting in the formation of a hitherto unreported dirhodium-η^1-allyl species postulated to serve as the active allylating agent in the reaction (Scheme 3). However, they were able to detect neither a cationic complex nor a metal-allyl intermediate, and thus, there has been a lack of consolidated mechanistic understanding for this transformation. Numerous similar reports of carbene insertion and allylic alkylation relay utilizing this strategy have followed thereafter,[7] making it necessary to establish the mechanistic details of this reaction. Recently, this strategy of ligand-induced dirhodium catalyst modification has also been applied to a carbonyl arylation reaction involving external chiral ligands.[8] This arylation reaction, supposedly proceeding via a similar modified catalyst, provides the motivation for developing asymmetric versions for MCRs as well. Since there are no experimental or computational reports on the mechanistic front for this intriguing MCR, in this work, we attempt to delineate its mechanism and the key species involved via computational and experimental studies.

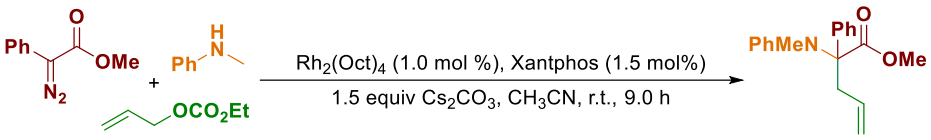

Scheme 2. General scheme for the synthesis of α-quaternary α-amino ester.

The reaction under investigation involves a relay pathway where the N–H insertion product (an α-amino ester) is formed, exits the catalytic cycle, and enters the subsequent catalytic cycle for allylic alkylation (Scheme 3). As shown by Wang and co-workers,[4] when the N–H insertion product is subjected to the standard reaction conditions, the α-quaternary α-amino ester is formed in high yield, thus confirming the relay nature of this MCR. This relay reactivity differs from the other MCRs where the ylide/enol intermediate traps the external electrophile. Under these circumstances, there is competition between the formation of the

two- and three-component products. However, in this case, the two-component product is first formed, which then undergoes further reaction. In the absence of the Xantphos ligand, the reaction stops at the N–H insertion product, thereby indicating that the ligand is essential for the subsequent allylic alkylation. Despite several recent reports using this strategy, the exact role of Xantphos has not been clearly understood. This has directly affected the development of asymmetric reactions. We therefore set out to investigate the role of Xantphos in the allylic alkylation of the α-amino ester. In this study, we provide the first explanation for the unique reactivity of the dirhodium/Xantphos system. The primary goal is to establish the nature of the electrophilic and nucleophilic species participating in this allylic alkylation reaction. We confirm our mechanistic model obtained through DFT calculations using *in situ* NMR and CV experiments.

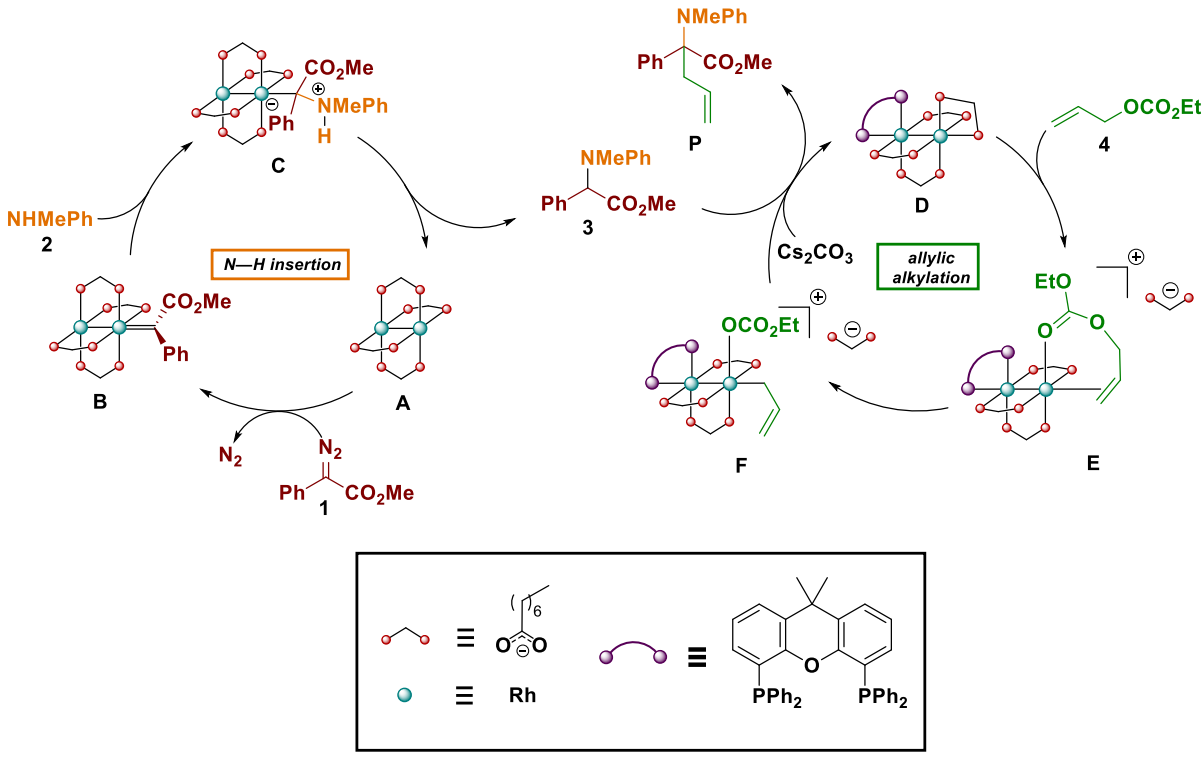

Scheme 3. Proposed mechanism for dirhodium tetracarboxylate/Xantphos-catalyzed carbene insertion and allylic alkylation relay.

2 Results and Discussion

2.1 Determining the reactive components

We begin our study by looking at the different possibilities for the most stable (resting) form of the catalyst (Figure 1) at the $SMD_{(acetonitrile)}$/B3LYP-D3(BJ)/6-311++G(d,p),SDD(Rh,Cs)//B3LYP-D3(BJ)/6-31G(d,p),SDD(Rh,Cs) level of theory. Considering several possibilities involving interactions with different species present in solution, in the absence and presence of Xantphos, we found **A4** and **D4** to respectively be the most likely resting states of the catalyst.[9]

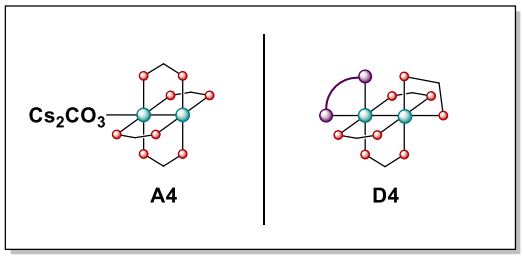

Figure 1. Resting forms of the catalyst in the absence (left) and presence (right) of Xantphos ligand.

With the resting states of the catalytic species in the absence and presence of the external Xantphos ligand established, we attempted to study the allylic alkylation of the N–H insertion product, *i.e.*, the α-aminoester **3** (Scheme 3). The mechanism of X–H (X = N, O, S, C) insertion reactions catalyzed by dirhodium tetracarboxylate and other transition metal complexes have been well studied computationally and reported to proceed through the formation of the metallocarbene, **B** from diazoesters followed by a nucleophilic addition to yield the ylide, **C** and subsequent proton transfer to yield the X–H insertion product, **3** (Scheme 3).[10] Therefore, the first catalytic cycle for the N–H insertion reaction leading to the α-aminoester, **3** has not been investigated in this work. The subsequent allylic alkylation cycle poses several questions where the nature of both the electrophile and nucleophile is

unclear. The nucleophile in this process is likely an enolate formed by the deprotonation of the α-proton of the α-aminoester by Cs_2CO_3. The enolization of the α-aminoester by Cs_2CO_3 in acetonitrile was confirmed by 42% deuterium incorporation using D_2O, as verified from ^1H NMR.[11] This enolization was calculated to proceed with a free energy barrier of 7.8 kcal mol^{-1} and 8.9 kcal mol^{-1} to form the (*E*)-enolate and (*Z*)-enolate respectively, thereby confirming the feasibility of such a process. All calculations presented hereafter have considered the kinetically more feasible (*E*)-enolate (calculations with the (*Z*)-enolate show similar trends[12]).

2.2 Reaction pathways in the absence of Xantphos

We first examined the pathway in the absence of the external ligand, Xantphos, to understand why the reaction stops at the N–H insertion product. In the absence of Xantphos, we considered a Rh-associated enolate (**H**) as a possible intermediate effecting a nucleophilic attack on allyl carbonate. We also speculated the external attack of a nucleophile on a Rh-associated allyl carbonate (**G**). However, whether the nucleophile (generated by a proton abstraction from the N–H insertion product) is a Cs-enolate or a Cs-free enolate is dubious. The nucleophilic attack of the Cs-enolate on the Rh-associated allyl carbonate $\mathbf{TS^{A4}(G\text{-}P)_{Cs}}$ was found to have a barrier of 23.1 kcal mol^{-1}, and the nucleophilic attack of the Rh-associated Cs-enolate on allyl carbonate $\mathbf{TS^{A4}(H\text{-}P)_{Cs}}$ to have a barrier of 22.6 kcal mol^{-1} (Figure 2, left). Such low free energy barriers generally indicate a facile reaction at room temperature (for reference, N_2 expulsion for metallocarbene formation, the typical rate-determining step for the N–H insertion pathway, has barriers of 22.3 kcal mol^{-1} and 14.7 kcal mol^{-1} with and without Xantphos respectively[13]), in stark contrast to experimental results where no allylic alkylation is observed in the absence of Xantphos.

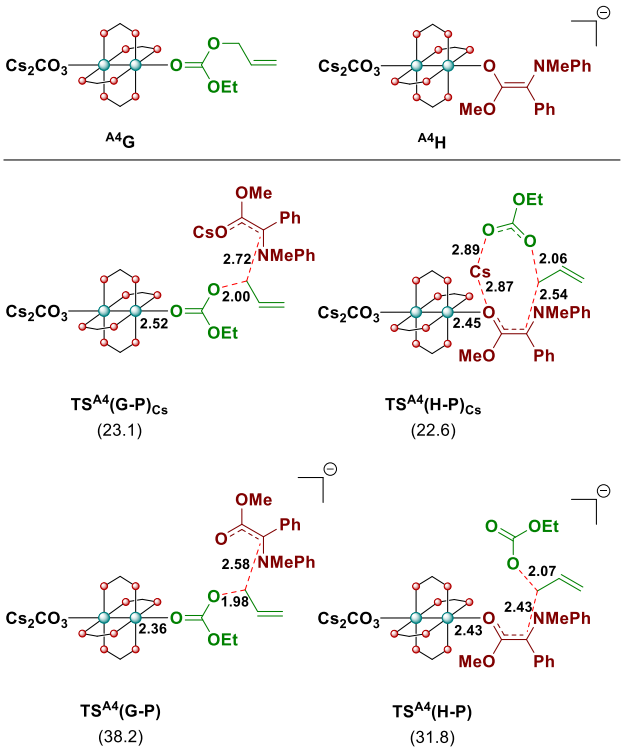

Figure 2. Transition states and the relative free energies (kcal mol^{-1}) with respect to the **A4** in the absence of Xantphos. All distances are in Å.

Previous studies on the extent of ion-pairing in alkali enolates have revealed a decreasing trend of ion-pairing going from Li^+ to Na^+ to K^+ ($\log K_{assoc} = 4.6, 3.3, 2.3$ respectively for diethyl malonate in DMSO) showing an inverse relation with cation size.[14] Based on the much larger size of the Cs^+ cation and the polarity of the solvent, the Cs-enolate is expected to be in the completely solvent-separated form. In fact, the so-called "cesium effect" used in justifying the enhanced reactivity of cesium salts, Cs_2CO_3 in particular, as compared to other alkali metal analogues is often explained in terms of the higher solubility of these salts on account of their greater solvation.[15] Thus, incorporating a Cs-enolate species in our DFT calculations might be incorrect, leading to the unrealistically low free energy barriers stated above. We, therefore, excluded the Cs-bound enolate from our calculations, and incorporated the Cs-free enolate as the nucleophilic species in this reaction and found the nucleophilic attack of the enolate on the Rh-associated allyl carbonate **TS^{A4}(G-P)** to have a barrier of 38.2

kcal mol^{-1} and that of the Rh-associated enolate on allyl carbonate **TS^{A4}(H-P)** to have a barrier of 31.8 kcal mol^{-1} (Figure 2, left). Such high free energy barriers explain why the reaction cannot proceed at room temperature in the absence of Xantphos.

2.3 Reaction pathways in the presence of Xantphos

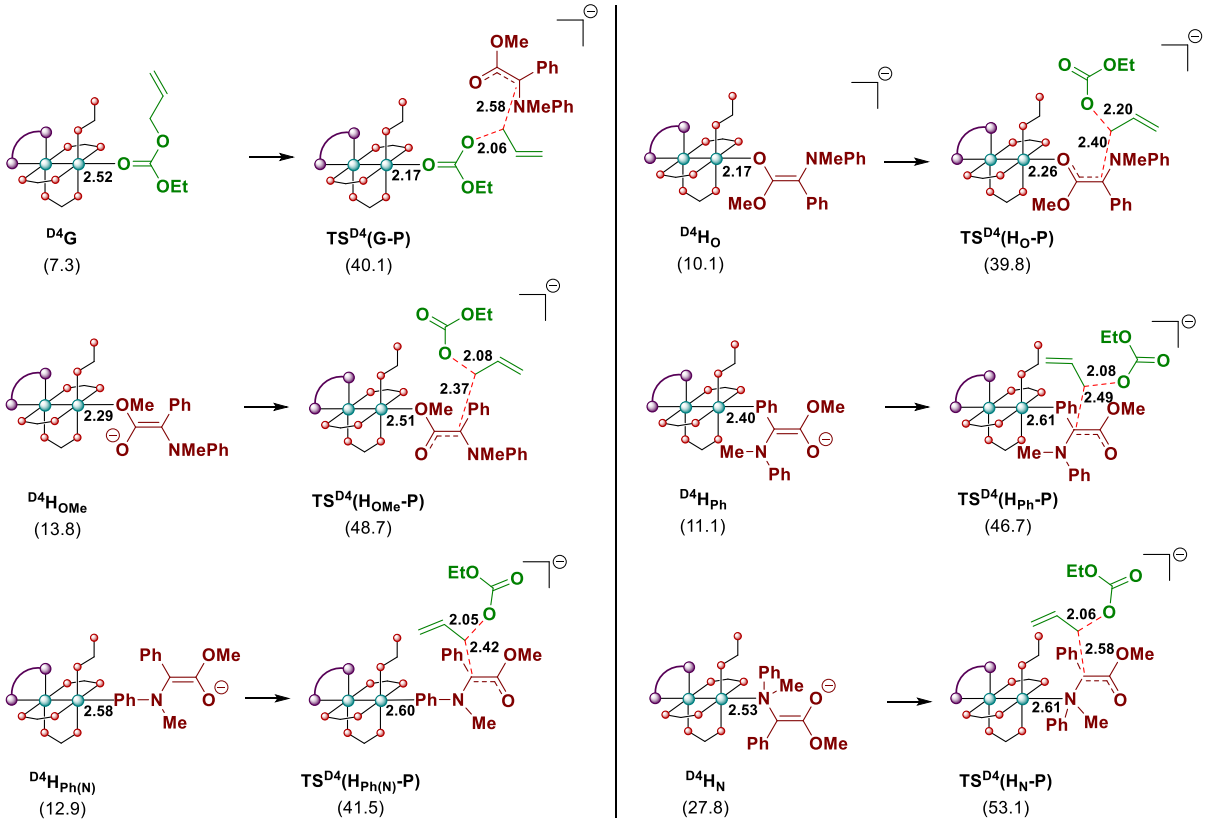

Figure 3. Intermediates and transition states and their associated free energies for pathways involving Rh-associated allyl carbonate and Rh-associated enolates in presence of Xantphos (free energies relative to catalyst **D4** are given in kcal mol^{-1}). All distances are in Å.

Having rationalized the reactivity in the absence of Xantphos, we investigated the potential reaction pathways in the presence of Xantphos (Figure 3). As discussed in Section 2.1, complex **D4** with a κ^2-Xantphos coordination is considered to be the most stable form of the catalyst,[16] and all relative free energies are hereafter referenced to it. As oxidative addition[4] has no literature precedence in the context of dirhodium catalysis, we looked at the possibility

of a Rh-associated enolate as an intermediate with a subsequent nucleophilic attack on allylic carbonate. Each of these pathways **TS^{D4}(Hx-P)** (where **X** denotes the enolate binding site) was calculated to have a preventively high free energy barrier. The nucleophilic attack of the enolate on the Rh-associated allyl carbonate **TS^{D4}(G-P)** was also found to have a very high barrier.[17] The possibility of an allyl transfer from an Rh-associated allyl carbonate to the neighboring κ^1-octanoate was also excluded based on high energy transition states.[18] Therefore, these conventional modes of reactivity fail to describe the allylic alkylation process.

2.4 Invoking oxidative addition

Wang and co-workers have hypothesized the complete dissociation of the octanoate ligand from the κ^2-Xantphos dirhodium tetracarboxylate complex along with a concomitant association of the allyl carbonate to the cationic dirhodium species (Scheme 3).[4,16] Previous reports involving dirhodium carboxylate catalysts with and without external ligands have also hypothesized the complete dissociation of a carboxylate ligand[19] although the external ligand-free version has been challenged.[20] We calculated the allyl carbonate associated dirhodium cation/octanoate ion pair **E** to be destabilized by 15.8 kcal mol^{-1} (Figure 4). However, the calculation of charged species, especially for an ion pair such as this, by even state-of-the-art DFT methods, has been previously noted to have errors up to five kcal mol^{-1} in general[21] and more than seven kcal mol^{-1} in certain cases.[22] In order to get a more accurate estimate, as outlined in previous protocols,[22] we tried incorporating up to four explicit solvent (MeCN) molecules without seeing any additional stabilization. A solvent phase optimization at the $SMD_{acetonitrile}$/B3LYP-D3(BJ)/6-311++G(d,p),SDD(Rh,Cs)//$SMD_{acetonitrile}$/B3LYP-D3(BJ)/6-31G(d,p),SDD(Rh,Cs) level of theory led to a reduced free energy of 14.1 kcal mol^{-1}.[23]

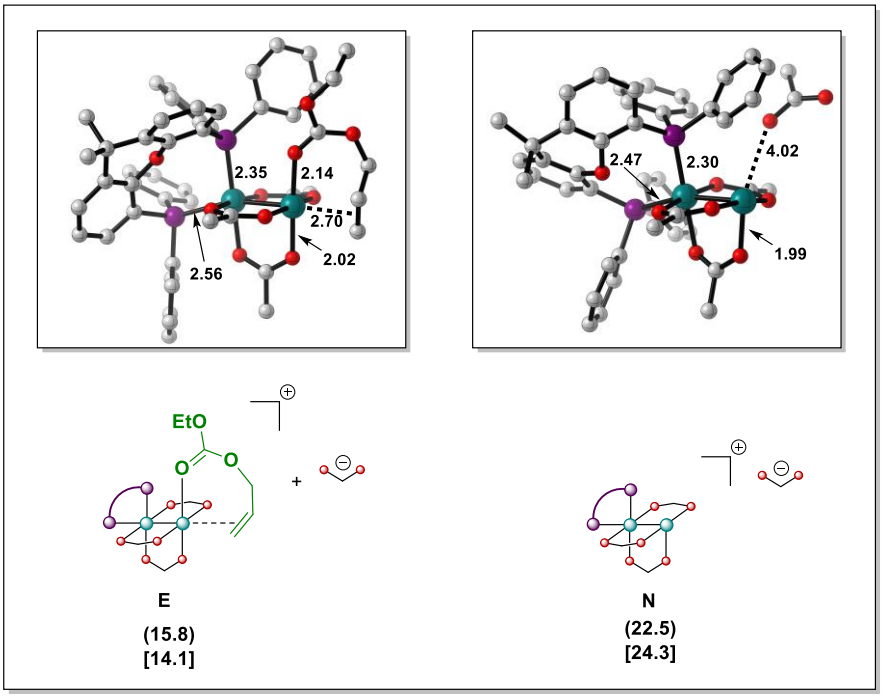

Figure 4. Optimized geometries for the ion pairs following the complete octanoate dissociation with and without allyl carbonate association (free energies in parenthesis correspond to the gas-phase optimized geometry relative to **D4**, free energies in square brackets correspond to the solvent-phase optimized geometry relative to **D4**, given in kcal mol^{-1}; H atoms have been omitted for clarity). All distances are in Å.

To ascertain the existence of such an intermediate, we therefore resorted to experimental methods. We first performed *in situ* ^{1}H NMR experiments (Figure 5) under inert conditions. Upon addition of the commercially available allyl chloride to a mixture of dirhodium tetraacetate and Xantphos in acetonitrile-d_3, we observed an allyl species distinct from the allyl chloride to be present in 16-20% relative yield (Figure 5(b)), which is absent in the control experiment without Xantphos (Figure 5(a)). Closer inspection revealed the allylic protons in the new allyl species to be in the form of a doublet of doublet of doublets at 4.41 ppm likely due to $^{3}J_{H\text{-}H}$ and $^{2}J_{H\text{-}Rh_1}$, and $^{3}J_{H\text{-}Rh_2}$ coupling corresponding to $^{103}Rh_2$–$^{103}Rh_1$ (J = 4.9 Hz, 6.9 Hz, 16.9 Hz) (Figure 5(c)), thereby suggesting the presence of a dirhodium-η^1-allyl species in solution.

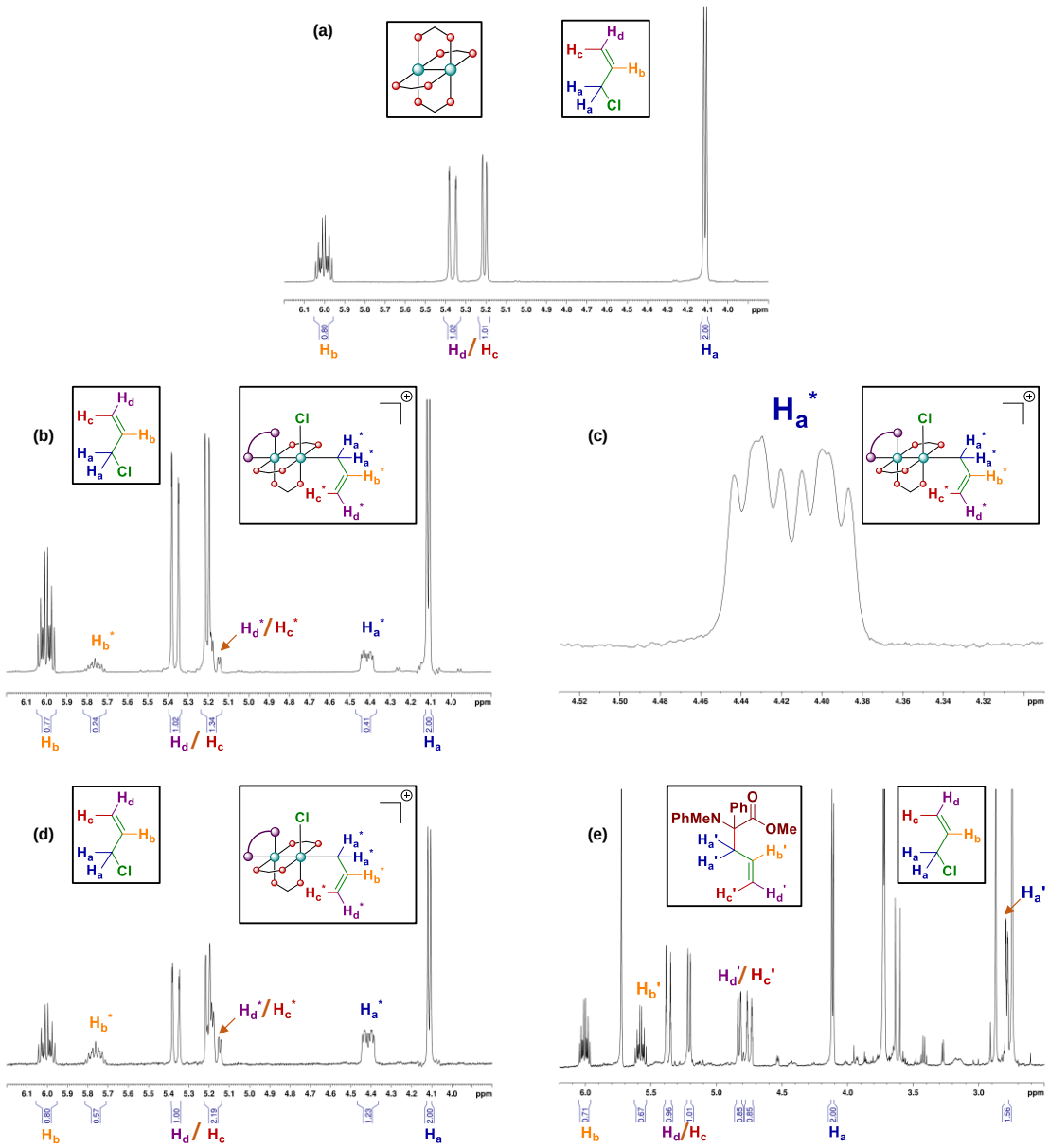

Figure 5. *in situ* ^{1}H NMR spectra of (a) equimolar mixture of dirhodium tetraacetate and allyl chloride (b) equimolar mixture of dirhodium tetraacetate, Xantphos, and allyl chloride (c) spectrum (b) magnified to focus on the doublet of doublet of doublet at 4.41 ppm (d) equimolar mixture (stirred overnight) of dirhodium tetraacetate, Xantphos, allyl chloride, and Cs_2CO_3 (1.5 equiv) (e) 1 equiv of α-amino ester added to the solution in (d); all in acetonitrile-d_3. **Note:** Although the cartoon representation adopted here is the same as before,

the rhodium complex being used here is dirhodium tetraacetate and not dirhodium tetraoctanoate.

This indicates the oxidative addition of the allylating agent (allyl carbonate, allyl chloride, etc.) across the rhodium center to which it is associated (in intermediate **E**) to form the detected dirhodium-η^1-allyl intermediate. Encouraged by this observation, we attempted to computationally examine the pathway of formation of this dirhodium-η^1-allyl intermediate (Figure 6). As the energy penalty of the ion pair **E** with respect to the neutral system cannot be accurately captured by our calculations (*vide supra*), we consider all subsequent free energies relative to this intermediate. The oxidative addition step **TS(E-F)** was found to be most favorable, possessing an activation free energy barrier of 17.2 kcal mol^{-1} with respect to the intermediate **E**, leading to the dirhodium-η^1-allyl intermediate **F** with a free energy of 14.9 kcal mol^{-1} with respect to **E**.[24] It must be noted here that the Rh "enyl" intermediate **K** (proposed by Evans and co-workers[25] in the case of Rh(I)/Rh(III) catalysis) was calculated to be 28.7 kcal mol^{-1} higher in energy than the dirhodium-η^1-allyl intermediate **F** and was therefore discarded as a possible intermediate. Additionally, the direct Rh-allylation by allyl carbonate (formally a *nucleophilic displacement*) was calculated to have a preventively high barrier.[18] For the sake of completeness, we also considered the exchange of the non-bridging octanoate ligand with the enolate and a subsequent inner sphere allylic alkylation by an Rh-associated allyl carbonate but found these steps to possess insurmountable barriers.[26]

In order to confirm that the oxidative addition step indeed takes place, CV (cyclic voltammetry) measurements were performed under inert conditions in acetonitrile with tertbutylammonium hexafluorophosphate as the supporting electrolyte (see Section **2.3** for details). Dirhodium tetraacetate showed the reported reversible one-electron oxidation/reduction wave at 1.18 V (Figure 7(a) and 7(b)),[27] while Xantphos exhibited three separate quasireversible oxidation/reduction waves at 1.13 V, 1.48 V, and 1.98 V.[28] When

dirhodium tetraacetate and Xantphos were taken together in solution, a nearly irreversible hump near 0.94 V was observed and the wave corresponding to one-electron oxidation/reduction of dirhodium tetraacetate turned quasireversible without any shift in potential (Figure 7(c) and 7(d)). This further supported our hypothesis of the complexation of Xantphos with dirhodium tetraacetate. Upon adding allyl chloride along with dirhodium tetraacetate and Xantphos in solution, new quasireversible reduction/oxidation waves near -1.38 V and -1.58 V were observed (Figure 7(e) and 7(f)), likely corresponding to the two-electron reduction of the oxidative addition product, i.e., $[Rh_2]^{6+}$ to $[Rh_2]^{4+}$. These waves were absent in all control experiments.[28] Thus, CV measurements validated that the product observed through *in situ* ^{1}H NMR results from oxidative addition.

Following the verification of the existence of the dirhodium-η^1-allyl intermediate and establishing the pathway of its formation, we turned to examine its fate in the presence of the α-amino ester. We performed the *in situ* ^{1}H NMR of a mixture of dirhodium tetraacetate, Xantphos, Cs_2CO_3, and allyl chloride in acetonitrile-*d3*, shaking the solution overnight to ensure maximum formation of the desired dirhodium-η^1-allyl complex. The ^{1}H peaks corresponding to the dirhodium-η^1-allyl species were reproduced, indicating 38-40% relative yield (Figure 5(d)). Upon addition of the α-amino ester, the aforementioned peaks disappear completely, and a new set of allyl peaks appear, corresponding to the product, i.e., α-quaternary α-amino ester (Figure 5(e)). This further validates the idea that this dirhodium-η^1-allyl intermediate, in fact, leads to product formation by the nucleophilic attack of the deprotonated α-amino ester.

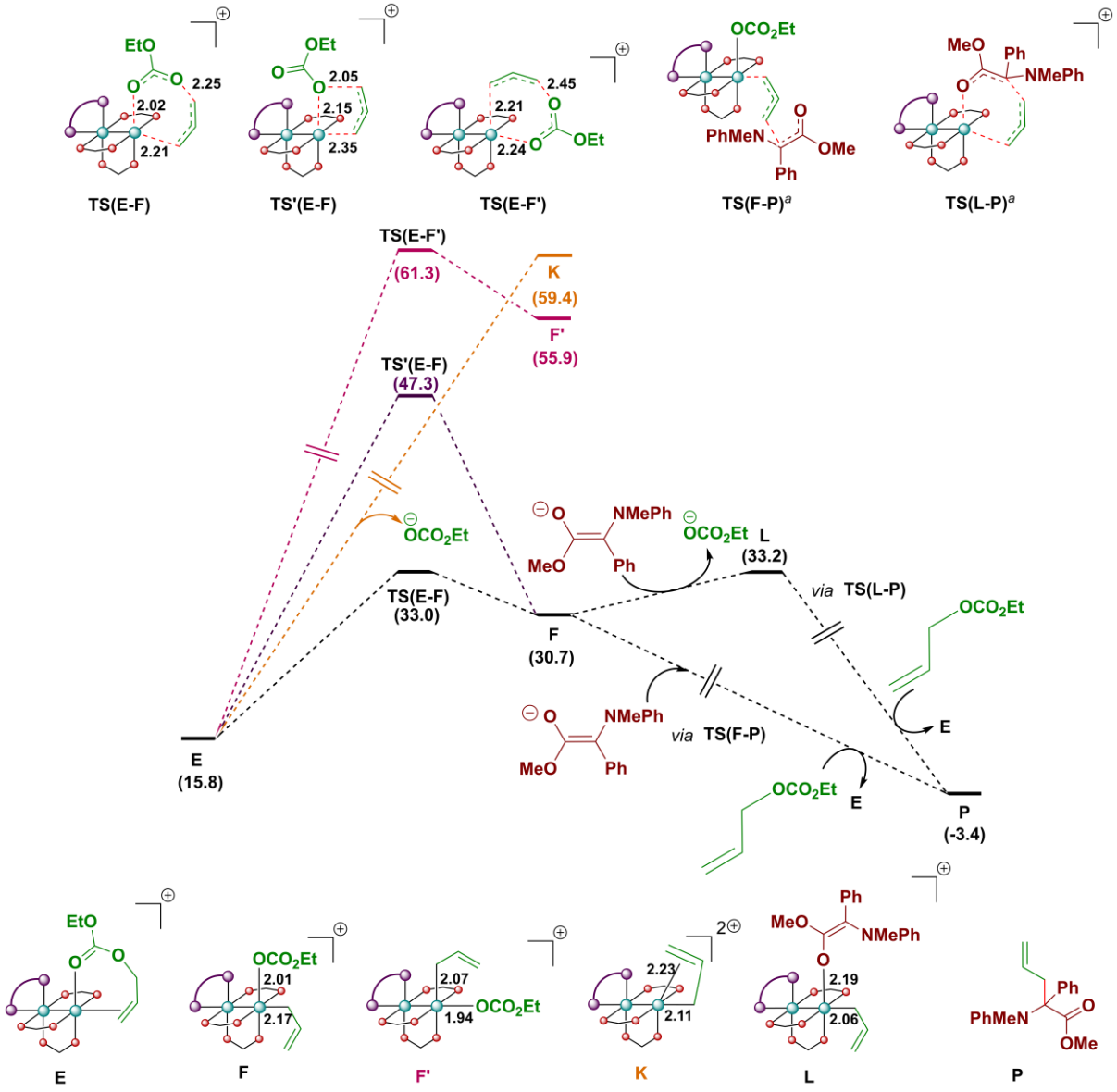

Figure 6. Free energy profile for the possible oxidative addition steps of allyl carbonate (free energies relative to **D4** are given in kcal mol^{-1}). [a] **TS(F-P)** and **TS(L-P)** are only representative; they could not be located. However, **TS(F-P)** is expected to be barrierless. All distances are in Å.

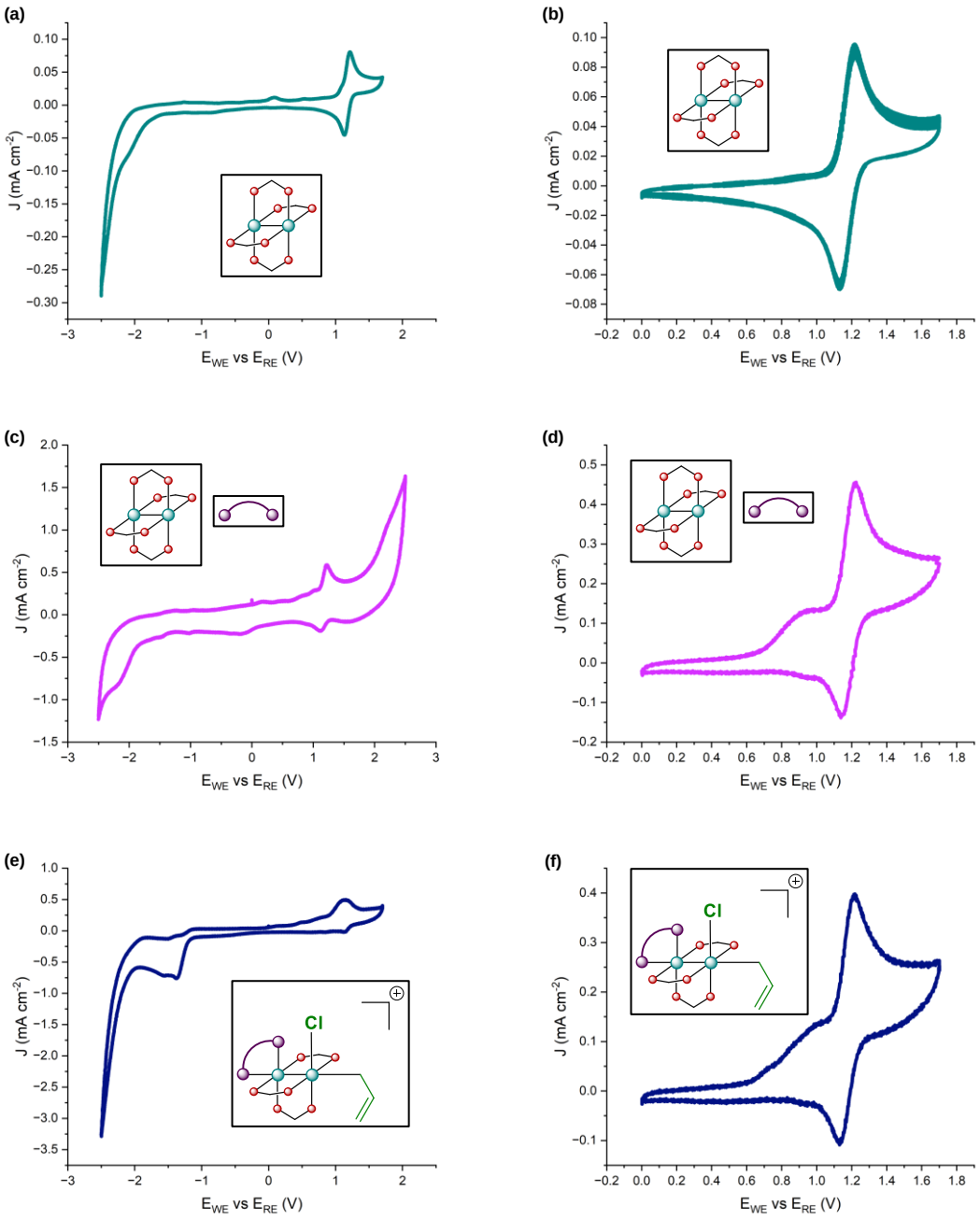

Figure 7. CV of (a), (b) dirhodium tetraacetate (c), (d) equimolar mixture of dirhodium tetraacetate and Xantphos (e), (f) equimolar mixture of dirhodium tetraacetate, Xantphos, and allyl chloride (1.25 mM in 0.1 M tetrabutylammonium hexafluorophosphate in CH_3CN; scan rate = 0.1 V s^{-1}). **Note:** Although the cartoon representation adopted here is the same as before, the rhodium complex being used here is dirhodium tetraacetate and not dirhodium tetraoctanoate.

Two possibilities for allylic alkylation of the α-amino ester through this dirhodium-η^1-allyl species are most likely (Figure 6) – (1) the external nucleophilic attack of the enolate, here an S_N2'-like attack via **TS(F-P)** is likely favored over an S_N2-like attack, as indicated by the deuterium labelling experiments by Wang and co-workers[4] as well as previous reports for rhodium based allylic alkylation reacitons;[29] (2) the exchange of the κ^1-octanoate with the enolate (**L**) followed by a reductive elimination via **TS(L-P)** to yield the α-quaternary α-amino ester. However, numerous attempts to locate the transition states for both the S_N2'-like and reductive elimination pathways were unsuccessful. A previous DFT study by Sunoj and co-workers[30] indicates a nearly barrierless allylic alkylation transition state from a rhodium-η^3-allyl intermediate. We attempted to generate the potential energy surface for the S_N2'-like process using a reduced system (acetate in place of octanoate and two trimethyl phosphine molecules in place of Xantphos), but no saddle point was seen in the relaxed energy scan (Figure 8), indicating a nearly barrierless transition state for this reaction.

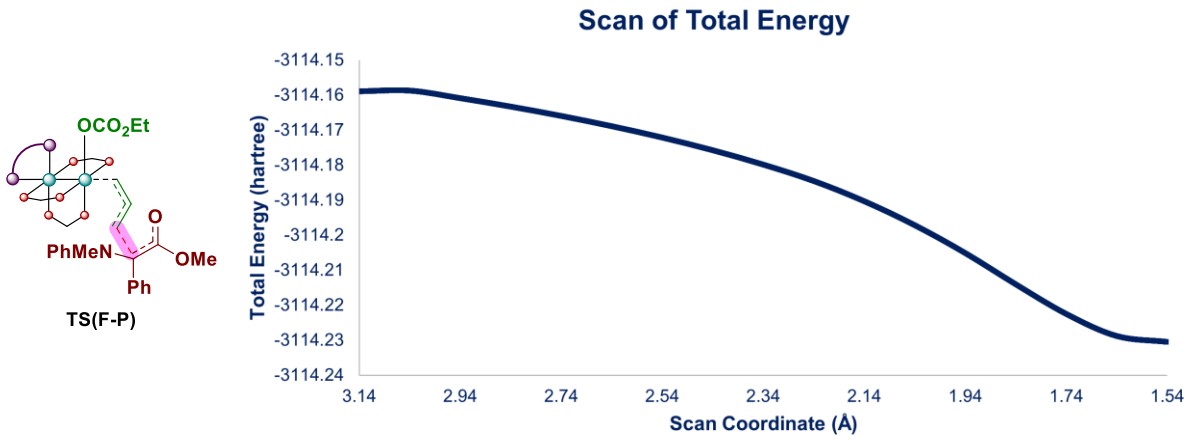

Figure 8. 1-dimensional Relaxed Potential Energy Surface (PES) scan. The distance being varied is highlighted in the representative **TS(F-P)**. Scan coordinate is in Å and Total Energy is in hartree.

The mechanism for the allylic alkylation pathway thus becomes clear (Figure 9) – the resting state of the catalyst **D4** is formed by the complexation of Xantphos with **A1**. The complete dissociation of the octanoate ligand from **D4** along with the concomitant association of the allyl carbonate forms the active catalyst for this pathway, **E**. Through a concerted oxidative addition process, the dirhodium-η^1-allyl intermediate **F** is generated, which serves as the allyl transfer agent in this reaction. A barrierless S_N2'-like nucleophilic attack of the deprotonated α-amino ester **3 (**in the Cs-free enolate form) results in the product **P** and the subsequent association of the allyl carbonate regenerates the active catalyst **E**. The energetic span of this pathway was calculated to be 17.2 kcal mol^{-1} (considering **E** to be the TDI and **TS(E-F)** to be the TDTS).[31]

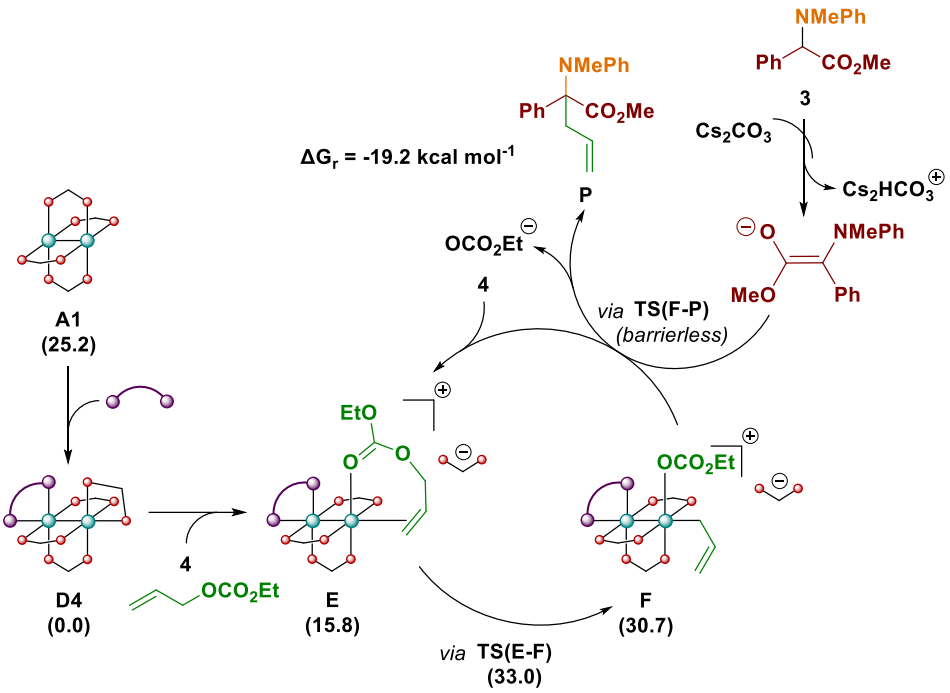

Figure 9. Mechanism for the allylic alkylation pathway (free energies relative to **D4** are given in kcal mol^{-1}).

3 Conclusion

In this work, we have unraveled the mechanistic possibilities for a dirhodium tetracarboxylate/Xantphos-catalyzed carbene insertion and allylic alkylation relay. For the first time, the existence of a dirhodium-η^1-allyl species as a reactive intermediate has been shown through computational studies, *in situ* NMR, and cyclic voltammetry experiments. The identity of the electrophilic and nucleophilic components in solution, *i.e.*, the dirhodium-η^1-allyl species and Cs-free enolate, has been resolved through a thorough investigation. This study also reveals the ability of dirhodium tetracarboxylate to undergo oxidative addition, resulting in the previously unknown Rh(II)–Rh(IV) mixed valence intermediate. This new mechanistic paradigm, enabled by the ability of Xantphos to completely dissociate a carboxylate bridge, is expected to have serious implications in inducing new modes of reactivity utilizing dirhodium tetracarboxylate catalysts. Confirmation of the κ^2-Xantphos dirhodium tetracarboxylate complex is anticipated to pave the way for utilizing chiral bulky external ligands for efficient stereoinduction at the axial position and expected to serve as a launchpad for the development of asymmetric reactions for achieving challenging transformations.

4 Methods

4.1 Computational Details

All calculations were done using Gaussian 16 suite of quantum chemical programs.[32] The hybrid density functional B3LYP[33] along with the D3(BJ) version of Grimme's dispersion correction was used for geometry optimization with 6-31G(d,p) basis set[34] for all atoms except Rh and Cs. For Rh and Cs, the SDD basis set with effective core potential (SDD) was chosen.[35] The stationary points were characterized by frequency calculations. The transition states were verified by the unique imaginary frequency calculation concerning the desired

reaction coordinate. Moreover, intrinsic reaction coordinate (IRC) calculations were carried out to verify the correctness of the transition states obtained. For all stationary points single calculations were performed using higher basis set 6-311++g(d,p) and all sorts of dispersion interaction were taken into account using the D3(BJ) version of Grimme's dispersion correction.[36] To take into the effect of solvent the keyword SCRF is used which performs calculations in the presence of a solvent by placing the solute in a cavity within the solvent reaction field, and herein solvent model density (SMD) with acetonitrile (ε = 35.688) was used.[37] The ZPE (zero point energy), thermal, and entropic corrections obtained at 298.15 K and 1 atm pressure calculated in the gas phase at B3LYP-D3(BJ)/6-31G(d,p),SDD(Rh,Cs) level of theory were added to the 'bottom-of-the-well' energies obtained from single point calculations at the $SMD_{acetonitrile}$/B3LYP-D3(BJ)/6-311++G(d,p),SDD(Rh,Cs) level of theory. All the values mentioned in this work, unless mentioned otherwise, correspond to free energies obtained at the $SMD_{acetonitrile}$/B3LYP-D3(BJ)/6-311++G(d,p),SDD(Rh,Cs)//B3LYP-D3(BJ)/6-31G(d,p),SDD(Rh,Cs) level of theory.

4.2 NMR Spectroscopy

^{1}H NMR spectra were measured on an Avance Bruker 500 MHz NMR spectrometer at rt. Chemical shifts were reported in ppm with respect to $SiMe_4$ by referencing the solvent peak to $SiMe_4$. All *in situ* NMR experiments were set up inside an N_2-filled glove box using an airtight screw cap NMR tube.

4.3 Cyclic Voltammetry

Cyclic Voltammetry was performed using 12 mL dried and distilled acetonitrile solutions containing 0.1 M tertbutylammonium hexafluorophosphate with 1.25 mM analyte under a nitrogen atmosphere. The electrodes consisted of a glassy carbon working electrode, a Pt wire counter electrode, and an Ag/AgCl reference electrode. Measurements were taken using a

Biologic SP-150 potentiostat. Prior to the measurement, all components of the analyte were taken inside the electrochemical cell and degassed before introducing it to nitrogen flow in order to ensure completely inert conditions.

4.4 Synthesis

The α-amino ester (**3**) was prepared according to a previously reported procedure.[38] All other chemicals were purchased commercially and used without further purification.

Acknowledgements

G. J. acknowledges the research grant (SPG/2021/003445) from the Science and Engineering Research Board (SERB). A. G. thanks the Dept. of Science & Technology, Govt. of India, for the KVPY fellowship. We are grateful to Prof. Balaji Rao Jagirdar, Prof. Santanu Mukherjee, and Dr. Veerabhadrarao Kaliginedi for generously allowing us to use their experimental labs and helpful discussions. We thank Ms. Kamla Devi Netam and Mr. Arko Seal for aiding in a portion of the experiments. We thank SERC, IISc for computing time.

References

(1) (a) Davies, H. M. L.; Manning, J. R. Catalytic C–H functionalization by metal carbenoid and nitrenoid insertion. *Nature* **2008**, *451*, 417-424. (b) Doyle, M. P.; Forbes, D. C. Recent Advances in Asymmetric Catalytic Metal Carbene Transformations. *Chem. Rev.* **1998**, *98*, 911-936. (c) Boyar, E. B.; Robinson, S. D. Rhodium(II) carboxylates. *Coord. Chem. Rev.* **1983**, *50*, 109-208. (d) Doyle, M. P.; Duffy, R.; Ratnikov, M.; Zhou, L. Catalytic Carbene Insertion into C−H Bonds. *Chem. Rev.* **2010**, *110*, 704-724. (e) Zhu, S.-F.; Zhou, Q.-L. Transition-Metal-Catalyzed Enantioselective Heteroatom–Hydrogen Bond Insertion Reactions. *Acc. Chem. Res.* **2012**, *45*, 1365-1377. (f) Gillingham, D.; Fei, N. Catalytic X–H insertion reactions based on carbenoids. *Chem. Soc. Rev.* **2013**, *42*, 4918-4931. (g) Davies, H.

M. L.; Beckwith, R. E. J. Catalytic Enantioselective C−H Activation by Means of Metal−Carbenoid-Induced C−H Insertion. *Chem. Rev.* **2003**, *103*, 2861-2904. (h) Davies, H. M. L. Finding Opportunities from Surprises and Failures. Development of Rhodium-Stabilized Donor/Acceptor Carbenes and Their Application to Catalyst-Controlled C–H Functionalization. *J. Org. Chem.* **2019**, *84*, 12722-12745. (i) Bulugahapitiya, P.; Landais, Y.; Parra-Rapado, L.; Planchenault, D.; Weber, V. A Stereospecific Access to Allylic Systems Using Rhodium(II)−Vinyl Carbenoid Insertion into Si−H, O−H, and N−H Bonds. *J. Org. Chem.* **1997**, *62*, 1630-1641. (j) Sambasivan, R.; Ball, Z. T. Metallopeptides for Asymmetric Dirhodium Catalysis. *J. Am. Chem. Soc.* **2010**, *132*, 9289-9291. (k) Hunter, A. C.; Chinthapally, K.; Sharma, I. Rh2(esp)2: An Efficient Catalyst for O–H Insertion Reactions of Carboxylic Acids into Acceptor/Acceptor Diazo Compounds. *Eur. J. Org. Chem.* **2016**, *2016*, 2260-2263.

(2) For reviews on dirhodium-catalyzed MCRs involving electrophile capture, see: (a) Guo, X.; Hu, W. Novel Multicomponent Reactions via Trapping of Protic Onium Ylides with Electrophiles. *Acc. Chem. Res.* **2013**, *46*, 2427-2440. (b) Zhang, D.; Hu, W. Asymmetric Multicomponent Reactions Based on Trapping of Active Intermediates. *Chem. Rec.* **2017**, *17*, 739-753. For articles on chiral Brønsted and Lewis acid catalyzed stereoselective reactions, see: (c) Xu, B.; Zhu, S.-F.; Zuo, X.-D.; Zhang, Z.-C.; Zhou, Q.-L. Enantioselective N–H Insertion Reaction of α-Aryl α-Diazoketones: An Efficient Route to Chiral α-Aminoketones. *Angew. Chem., Int. Ed.* **2014**, *53*, 3913-3916. (d) Saito, H.; Morita, D.; Uchiyama, T.; Miyake, M.; Miyairi, S. Cinchona alkaloids induce asymmetry in the insertion reaction of thermally generated carbenes into N−H bonds. *Tetrahedron Lett.* **2012**, *53*, 6662-6664. (e) Xu, B.; Zhu, S.-F.; Xie, X.-L.; Shen, J.-J.; Zhou, Q.-L. Asymmetric N–H Insertion Reaction Cooperatively Catalyzed by Rhodium and Chiral Spiro Phosphoric Acids. *Angew. Chem., Int. Ed.* **2011**, *50*, 11483-11486. (f) Maolin, Li.; Mengqing, C.; Bin, X.; Shoufei, Z.; Quilin,

Z.Enantioselective O—H Bond Insertion of α-Diazoketones with Alcohols Cooperatively Catalyzed by Achiral Dirhodium Complexes and Chiral Spiro Phosphoric Acids. *Acta Chim. Sinica* **2018**, *76*, 883-889. (g) Zhang, Y.; Yao, Y.; He, L.; Liu, Y.; Shi, L. Rhodium(II)/Chiral Phosphoric Acid-Cocatalyzed Enantioselective O–H Bond Insertion of α-Diazo Esters. *Adv. Synth. Catal.* **2017**, *359*, 2754-2761. (h) Tan, F.; Liu, X.; Hao, X.; Tang, Y.; Lin, L.; Feng, X. Asymmetric Catalytic Insertion of α-Diazo Carbonyl Compounds into O–H Bonds of Carboxylic Acids. *ACS Catal.* **2016**, *6*, 6930-6934. (i) Xu, B.; Zhu, S.-F.; Zhang, Z.-C.; Yu, Z.-X.; Ma, Y.; Zhou, Q.-L. Highly enantioselective S–H bond insertion cooperatively catalyzed by dirhodium complexes and chiral spiro phosphoric acids. *Chem. Sci.* **2014**, *5*, 1442-1448. (j) Yang, J.; Ke, C.; Zhang, D.; Liu, X.; Feng, X. Enantioselective Synthesis of 2,2,3-Trisubstituted Indolines via Bimetallic Relay Catalysis of α-Diazoketones with Enones. *Org. Lett.* **2018**, *20*, 4536-4539. For cooperative catalysis of rhodium and other metals, see: (k) Kang, Z.; Chang, W.; Tian, X.; Fu, X.; Zhao, W.; Xu, X.; Liang, Y.; Hu, W. Ternary Catalysis Enabled Three-Component Asymmetric Allylic Alkylation as a Concise Track to Chiral α,α-Disubstituted Ketones. *J. Am. Chem. Soc.* **2021**, *143*, 20818-20827. (l) Chen, Z.-S.; Huang, X.-Y.; Liu, Q.; Song, D.-X.; Yang, F.; Ji, K. Three-component chemo-selective oxy-allylation of α-diazo carbonyl compounds: Access to α-ternary carboxylic esters. *Journal of Catalysis* **2023**, *417*, 52-59. (m) Yuan, W.; Eriksson, L.; Szabó, K. J. Rhodium-Catalyzed Geminal Oxyfluorination and Oxytrifluoro-Methylation of Diazocarbonyl Compounds. *Angew. Chem., Int. Ed.* **2016**, *55*, 8410-8415.

(3) For a review of transition-metal-catalyzed allylic alkylation reactions, see: (a) Trost, B. M.; Crawley, M. L. Asymmetric Transition-Metal-Catalyzed Allylic Alkylations: Applications in Total Synthesis. *Chem. Rev.* **2003**, *103*, 2921-2944. (b) For a review of palladium-catalyzed allylic alkylation reactions, see: Pàmies, O.; Margalef, J.; Cañellas, S.; James, J.; Judge, E.; Guiry, P. J.; Moberg, C.; Bäckvall, J.-E.; Pfaltz, A.; Pericàs, M. A.;

Diéguez, M. Recent Advances in Enantioselective Pd-Catalyzed Allylic Substitution: From Design to Applications. *Chem. Rev.* **2021**, *121*, 4373-4505. (c) For a review of rhodium-catalyzed allylic alkylation reactions, see: Thoke, M. B.; Kang, Q. Rhodium-Catalyzed Allylation Reactions. *Synthesis* **2019**, *51*, 2585-2631. (d) Minami, I.; Shimizu, I.; Tsuji, J. Reactions of allylic carbonates catalyzed by palladium, rhodium, ruthenium, molybdenum, and nickel complexes; allylation of carbonucleophiles and decarboxylation- dehydrogenation. *J. Organomet. Chem.* **1985**, *296*, 269-280. For a review of iridium-catalyzed allylic alkylation reactions, see: (e) Cheng, Q.; Tu, H.-F.; Zheng, C.; Qu, J.-P.; Helmchen, G.; You, S.-L. Iridium-Catalyzed Asymmetric Allylic Substitution Reactions. *Chem. Rev*. **2019**, *119*, 1855-1969.

(4) Lu, B.; Liang, X.; Zhang, J.; Wang, Z.; Peng, Q.; Wang, X. Dirhodium(II)/Xantphos-Catalyzed Relay Carbene Insertion and Allylic Alkylation Process: Reaction Development and Mechanistic Insights. *J. Am. Chem. Soc.* **2021**, *143*, 11799-11810.

(5) (a) Davies, H. M. L.; Morton, D. Guiding principles for site selective and stereoselective intermolecular C–H functionalization by donor/acceptor rhodium carbenes. *Chem. Soc. Rev.* **2011**, *40*, 1857-1869. (b) Davies, H. M. L.; Liao, K. Dirhodium tetracarboxylates as catalysts for selective intermolecular C–H functionalization. *Nat. Rev. Chem.* **2019**, *3*, 347-360. (c) Liao, K.; Negretti, S.; Musaev, D. G.; Bacsa, J.; Davies, H. M. L. Site-selective and stereoselective functionalization of unactivated C–H bonds. *Nature* **2016**, *533*, 230-234. (d) DeAngelis, A.; Shurtleff, V. W.; Dmitrenko, O.; Fox, J. M. Rhodium(II)-Catalyzed Enantioselective C−H Functionalization of Indoles. *J. Am. Chem. Soc.* **2011**, *133*, 1650-1653. (e) Li, Z.; Davies, H. M. L. Enantioselective C−C Bond Formation by Rhodium-Catalyzed Tandem Ylide Formation/[2,3]-Sigmatropic Rearrangement between Donor/Acceptor Carbenoids and Allylic Alcohols. *J. Am. Chem. Soc.* **2010**, *132*, 396-401. (f) Davies, H. M. L.; Hansen, T.; Rutberg, J.; Bruzinski, P. R. Rhodium(II) (S)-N-(arylsulfonyl)prolinate

catalyzed asymmetric insertions of vinyl- and phenylcarbenoids into the Si–H bond. *Tetrahedron Lett.* **1997**, *38*, 1741-1744. (g) Zhou, C.-Y.; Wang, J.-C.; Wei, J.; Xu, Z.-J.; Guo, Z.; Low, K.–H.; Che, C.-M. Dirhodium Carboxylates Catalyzed Enantioselective Coupling Reactions of α-Diazophosphonates, Anilines, and Electron-Deficient Aldehydes. *Angew. Chem., Int. Ed.* **2012**, *51*, 11376-11380.

(6) (a) Trindade, A. F.; Coelho, J. A. S.; Afonso, C. A. M.; Veiros, L. F.; Gois, P. M. P. Fine Tuning of Dirhodium(II) Complexes: Exploring the Axial Modification. *ACS Catal.* **2012**, *2*, 370-383. (b) Hong, B.; Shi, L.; Li, L.; Zhan, S.; Gu, Z. Paddlewheel dirhodium(II) complexes with N-heterocyclic carbene or phosphine ligand: New reactivity and selectivity. *Green Synthesis and Catalysis* **2022**, *3*, 137-149. (c) Sambasivan, R.; Zheng, W.; Burya, S. J.; Popp, B. V.; Turro, C.; Clementi, C.; Ball, Z. T. A tripodal peptide ligand for asymmetric Rh(ii) catalysis highlights unique features of on-bead catalyst development. *Chem. Sci.* **2014**, *5*, 1401-1407. (d) Sarkar, M.; Daw, P.; Ghatak, T.; Bera, J. K. Amide-Functionalized Naphthyridines on a RhII–RhII Platform: Effect of Steric Crowding, Hemilability, and Hydrogen-Bonding Interactions on the Structural Diversity and Catalytic Activity of Dirhodium(II) Complexes. *Chem. Eur. J.* **2014**, *20*, 16537-16549. (e) Anderson, B. G.; Cressy, D.; Patel, J. J.; Harris, C. F.; Yap, G. P. A.; Berry, J. F.; Darko, A. Synthesis and Catalytic Properties of Dirhodium Paddlewheel Complexes with Tethered, Axially Coordinating Thioether Ligands. *Inorg. Chem.* **2019**, *58*, 1728-1732. (f) Cressy, D.; Zavala, C.; Abshire, A.; Sheffield, W.; Darko, A. Tuning Rh(II)-catalysed cyclopropanation with tethered thioether ligands. *Dalton Transactions* **2020**, *49*, 15779-15787. (g) Zavala, C.; Darko, A. Effect of Tethered, Axially Coordinated Ligands (TACLs) on Dirhodium(II,II) Catalyzed Cyclopropanation: A Linear Free Energy Relationship Study. *J. Org. Chem.* **2022**, *87*, 6910-6917. (h) Kisan, H. K.; Sunoj, R. B. Axial Coordination Dichotomy in Dirhodium Carbenoid Catalysis: A Curious Case of Cooperative Asymmetric Dual-Catalytic Approach

toward Amino Esters. *J. Org. Chem.* **2015**, *80*, 2192–2197. (i) Laconsay, C. J.; Pla-Quintana, A.; Tantillo, D. J. Effects of Axial Solvent Coordination to Dirhodium Complexes on the Reactivity and Selectivity in C–H Insertion Reactions: A Computational Study. *Organometallics* **2021**, *40*, 4120-4132.

(7) (a) Yang, Y.; Lu, B.; Xu, G.; Wang, X. Overcoming O–H Insertion to Para-Selective C–H Functionalization of Free Phenols: Rh(II)/Xantphos Catalyzed Geminal Difunctionalization of Diazo Compounds. *ACS Cent. Sci.* **2022**, *8*, 581-589. (b) Zhang, J.; Lu, B.; Ge, Z.; Wang, L.; Wang, X. Selective Construction of All-Carbon Quaternary Centers via Relay Catalysis of Indole C–H Functionalization/Allylic Alkylation. *Org. Lett.* **2022**, *24*, 8423-8428. (c) Ge, Z.; Lu, B.; Teng, H.; Wang, X. Efficient Synthesis of Diaryl Quaternary Centers by Rh(II)/Xantphos Catalyzed Relay C−H Functionalization and Allylic Alkylation. *Chem. Eur. J.* **2023**, *29*, e202202820.

(8) Shi, L.; Xue, X.; Hong, B.; Li, Q.; Gu, Z. Dirhodium(II)/Phosphine Catalyst with Chiral Environment at Bridging Site and Its Application in Enantioselective Atropisomer Synthesis. *ACS Cent. Sci.* 2023. https://doi.org/10.1021/acscentsci.2c01207

(9) See Supporting Information Section A.

(10) (a) Hansen, J.; Autschbach, J.; Davies, H. M. L. Computational Study on the Selectivity of Donor/Acceptor-Substituted Rhodium Carbenoids. *J. Org. Chem.* **2009**, *74*, 6555-6563. (b) Liang, Y.; Zhou, H.; Yu, Z.-X. Why Is Copper(I) Complex More Competent Than Dirhodium(II) Complex in Catalytic Asymmetric O−H Insertion Reactions? A Computational Study of the Metal Carbenoid O−H Insertion into Water. *J. Am. Chem. Soc.* **2009**, *131*, 17783-17785. (c) Zhou, M.; Springborg, M. Theoretical study of the mechanism behind the site- and enantio-selectivity of C–H functionalization catalysed by chiral dirhodium catalyst. *Phys. Chem. Chem. Phys.* **2020**, *22*, 9561-9572.

(11) See Supporting Information Section C.

(12) See Supporting Information Figures S2 and S3 for details.

(13) See Supporting Information Figure S4.

(14) (a) Bastos, E. L. Acid–Base and Solvation properties of Metal Enolates. Part 1: The Enolate Ion and Main-Group Metal Enolates. In *PATAI'S Chemistry of Functional Groups*, **2017**, pp 1-54. (b) Olmstead, W. N.; Bordwell, F. G. Ion-pair association constants in dimethyl sulfoxide. *J. Org. Chem.* **1980**, *45*, 3299-3305.

(15) (a) Dijkstra, G.; Kruizinga, W. H.; Kellogg, R. M. An assessment of the causes of the "cesium effect". *J. Org. Chem.* **1987**, *52*, 4230-4234. (b) Kennedy, C. R.; Guidera, J. A.; Jacobsen, E. N. Synergistic Ion-Binding Catalysis Demonstrated via an Enantioselective, Catalytic [2,3]-Wittig Rearrangement. *ACS Cent. Sci.* **2016**, *2*, 416-423.

(16) See Figure S5 for the calculated reaction profile for the formation of the κ^2-Xantphos dirhodium tetracarboxylate complex **D4** and the complete dissociation of the octanoate ligand from **D4** followed along with the concomitant association of the allyl carbonate to form **E**.

(17) In both the above possibilities, incorporating a Cs-enolate or a Rh-associated Cs-enolate as the nucleophile yields much lower barriers, but must be rejected in accordance with our previous justification. See Supporting Information Figure S6 for details.

(18) See Supporting Information Figure S7 for details.

(19) (a) Lou, Y.; Horikawa, M.; Kloster, R. A.; Hawryluk, N. A.; Corey, E. J. A New Chiral Rh(II) Catalyst for Enantioselective [2 + 1]-Cycloaddition. Mechanistic Implications and Applications. *J. Am. Chem. Soc.* **2004**, *126*, 8916-8918. (b) Lou, Y.; Remarchuk, T. P.; Corey, E. J. Catalysis of Enantioselective [2+1]-Cycloaddition Reactions of Ethyl Diazoacetate and Terminal Acetylenes Using Mixed-Ligand Complexes of the Series Rh2(RCO2)n (L*4-n). Stereochemical Heuristics for Ligand Exchange and Catalyst Synthesis. *J. Am. Chem. Soc.* **2005**, *127*, 14223-14230. (c) Wang, C.; Zhou, Y.; Bao, X.

Mechanistic Insights into the Rh-Catalyzed Transannulation of Pyridotriazole with Phenylacetylene and Benzonitrile: A DFT Study. *J. Org. Chem.* **2017**, *82*, 3751-3759.

(20) Nowlan, D. T.; Singleton, D. A. Mechanism and Origin of Enantioselectivity in the Rh2(OAc)(DPTI)3-Catalyzed Cyclopropenation of Alkynes. *J. Am. Chem. Soc.* **2005**, *127*, 6190-6191.

(21) Liu, Z.; Patel, C.; Harvey, J. N.; Sunoj, R. B. Mechanism and reactivity in the Morita–Baylis–Hillman reaction: the challenge of accurate computations. *Phys. Chem. Chem. Phys.* **2017**, *19*, 30647-30657.

(22) Plata, R. E.; Singleton, D. A. A Case Study of the Mechanism of Alcohol-Mediated Morita Baylis–Hillman Reactions. The Importance of Experimental Observations. *J. Am. Chem. Soc.* **2015**, *137*, 3811-3826.

(23) See Supporting Information Tables S1 and S2 for a comparison of the gas phase and solvent phase optimized separated ion pair (**E**) energy at different levels of theory.

(24) Calculations using dirhodium tetraacetate and allyl chloride (which are used for all experiments) show similar trends. See Supporting Information Figure S8 for details.

(25) (a) Evans, P. A.; Nelson, J. D. Conservation of Absolute Configuration in the Acyclic Rhodium-Catalyzed Allylic Alkylation Reaction: Evidence for an Enyl ($\sigma + \pi$) Organorhodium Intermediate. *J. Am. Chem. Soc.* **1998**, *120*, 5581-5582. (b) Lawson, D. N.; Osborn, J. A.; Wilkinson, G. Interaction of tris(triphenylphosphine)chlororhodium(I) with iodomethane, methylallyl, and allyl chloride. *J. Chem. Soc. A* **1966**, 1733-1736. (c) Turnbull, B. W. H.; Evans, P. A. Asymmetric Rhodium-Catalyzed Allylic Substitution Reactions: Discovery, Development and Applications to Target-Directed Synthesis. *J. Org. Chem.* **2018**, *83*, 11463-11479.

(26) See Supporting Information Figure S9 for details.

(27) Zhu, T. P.; Ahsan, M. Q.; Malinski, T.; Kadish, K. M.; Bear, J. L. Electrochemical studies of a series of dirhodium(II) complexes with acetate and acetamidate bridging ligands. *Inorg. Chem.* **1984**, *23*, 2-3.

(28) See Supporting Information Figure S10.

(29) (a) van Haaren, R. J.; Zuidema, E.; Fraanje, J.; Goubitz, K.; Kamer, P. C. J.; van Leeuwen, P. W. N. M.; van Strijdonck, G. P. F. Synthesis and characterisation of bite angle-dependent (η1-allyl)Rh and (η3-allyl)Rh complexes bearing diphosphine ligands. Implications for nucleophilic substitution reactions. *C. R. Chimie* **2002**, *5*, 431-440. (b) Tsuji, J.; Minami, I.; Shimizu, I. Allyation of carbonucleophiles with allylic carbonates under neutral conditions catalyzed by rhodium complexes. *Tetrahedron Lett.* **1984**, *25*, 5157-5160.

(30) Pareek, M.; Sunoj, R. B. Mechanistic insights into rhodium-catalyzed enantioselective allylic alkylation for quaternary stereogenic centers. *Chem. Sci.* **2021**, *12*, 2527-2539.

(31) Kozuch, S.; Shaik, S. How to Conceptualize Catalytic Cycles? The Energetic Span Model. *Acc. Chem. Res.* **2011**, *44*, 101-110.

(32) Frisch, M. J.; Trucks, G. W.; Schlegel, H. B.; Scuseria, G. E.; Robb, M. A.; Cheeseman, J. R.; Scalmani, G.; Barone, V.; Petersson, G. A.; Nakatsuji, H.; Li, X.; Caricato, M.; Marenich, A. V.; Bloino, J.; Janesko, B. G.; Gomperts, R.; Mennucci, B.; Hratchian, H. P.; Ortiz, J. V.; Izmaylov, A. F.; Sonnenberg, J. L.; Williams-Young, D.; Ding, F.; Lipparini, F.; Egidi, F.; Goings, J.; Peng, B.; Petrone, A.; Henderson, T.; Ranasinghe, D.; Zakrzewski, V. G.; Gao, J.; Rega, N.; Zheng, G.; Liang, W.; Hada, M.; Ehara, M.; Toyota, K.; Fukuda, R.; Hasegawa, J.; Ishida, M.; Nakajima, T.; Honda, Y.; Kitao, O.; Nakai, H.; Vreven, T.; Throssell, K.; Montgomery, J. A.; Jr.; Peralta, J. E.; Ogliaro, F.; Bearpark, M. J.; Heyd, J. J.; Brothers, E. N.; Kudin, K. N.; Staroverov, V. N.; Keith, T. A.; Kobayashi, R.; Normand, J.; Raghavachari, K.; Rendell, A. P.; Burant, J. C.; Iyengar, S. S.; Tomasi, J.; Cossi, M.; Millam, J. M.; Klene, M.; Adamo, C.; Cammi, R.; Ochterski, J. W.; Martin, R. L.; Morokuma, K.;

Farkas, O.; Foresman, J. B.; Fox, D. J. *Gaussian 16, revision C.01;* Gaussian, Inc.: Wallingford CT, 2016.

(33) (a) Becke, A. D. Density-functional thermochemistry. III. The role of exact exchange. *J. Chem. Phys.* **1993**, *98*, 5648-5652. (b) Lee, C.; Yang, W.; Parr, R. G. Development of the Colle-Salvetti correlation-energy formula into a functional of the electron density. *Phys. Rev. B* **1988**, *37*, 785-789.

(34) (a) Hariharan, P. C.; Pople, J. A. The influence of polarization functions on molecular orbital hydrogenation energies. *Theoret. Chim. Acta* **1973**, *28*, 213-222. (b) Hehre, W. J.; Ditchfield, R.; Pople, J. A. Self—Consistent Molecular Orbital Methods. XII. Further Extensions of Gaussian—Type Basis Sets for Use in Molecular Orbital Studies of Organic Molecules. *J. Chem. Phys.* **1972**, *56*, 2257-2261.

(35) (a) Andrae, D.; Häußermann, U.; Dolg, M.; Stoll, H.; Preuß, H. Energy-adjusted ab initio pseudopotentials for the second and third row transition elements. *Theoret. Chim. Acta* **1990**, *77*, 123-141. (b) Fuentealba, P. On the reliability of semiempirical pseudopotentials: dipole polarisability of the alkali atoms. *J. Phys. B: Atom. and Mol. Phys.* **1982**, *15*, L555.

(36) Grimme, S.; Ehrlich, S.; Goerigk, L. *J. Comput. Chem*. **2011**, *32*, 1456-1465.

(37) Marenich, A. V.; Cramer, C. J.; Truhlar, D. G. Universal Solvation Model Based on Solute Electron Density and on a Continuum Model of the Solvent Defined by the Bulk Dielectric Constant and Atomic Surface Tensions. *J. Phys. Chem. B* **2009**, *113*, 6378-6396.

(38) Wang, Y.; Zhu, Y.; Chen, Z.; Mi, A.; Hu, W.; Doyle, M. P. A Novel Three-Component Reaction Catalyzed by Dirhodium(II) Acetate: Decomposition of Phenyldiazoacetate with Arylamine and Imine for Highly Diastereoselective Synthesis of 1,2-Diamines. *Org. Lett.* **2003**, *5*, 3923-3926.

TOC Graphics